Dalton Transactions

ROYAL SOCIETY OF CHEMISTRY

PAPER

View Article Online
View Journal | View Issue

Check for updates

Cite this: *Dalton Trans.*, 2021, **50**, 8057

Coordination chemistry of [2 + 2] Schiff-base macrocycles derived from the dianilines [(2-$NH_2C_6H_4)_2X$] (X = CH_2CH_2, O): structural studies and ROP capability towards cyclic esters†

Kuiyuan Wang,[a] Timothy J. Prior,[a] David L. Hughes,[b] Abdessamad Arbaoui[b] and Carl Redshaw *[a]

Received 2nd March 2021,
Accepted 4th May 2021

DOI: 10.1039/d1dt00711d

rsc.li/dalton

Reaction of the [2 + 2] Schiff-base macrocycles {[2-(OH)-5-(R)-C_6H_2-1,3-$(CH)_2$][CH_2CH_2(2-$C_6H_4N)_2$]}$_2$ (R = Me, L^1H_2; *t*Bu, L^2H_2) with $FeBr_2$ afforded the complexes [FeBr(L^1H_2)]$_2$[$(FeBr_3)_2$O]·2MeCN (**1**·2MeCN), [FeBr(L^2H_2)][X] (X = 0.5$(FeBr_3)_2$O, **2**·0.5MeCN, X = Br, **3**·5.5MeCN), respectively. Reaction of L^2H_2 with [KFe(O*t*Bu)$_3$(THF)] (formed *in situ* from $FeBr_2$ and KO*t*Bu), following work-up, led to the isolation of the complex [Fe(L^2)(L^2H)]·3MeCN (**4**·3MeCN), whilst with [$CuBr_2$] afforded [CuBr(L^2H_2)][$CuBr_2$]·2MeCN (**5**·2MeCN). Attempts to form mixed Co/Ti species by reaction of [CoBrL^2][$CoBr_3$(NCMe)] with $TiCl_4$ resulted in [L^2H_4][$CoBr_4$]·2MeCN (**6**·2MeCN). Use of the related oxy-bridged Schiff-base macrocycles {[2-(OH)-5-(R)-C_6H_2-1,3-$(CH)_2$][O(2-$C_6H_4N)_2$]}$_2$ (R = Me, L^3H_2; *t*Bu, L^4H_2) with $CoBr_2$ led to the isolation of the complexes [$(CoBr)_2(L^3)$]·2C_3H_6O (**7**·2C_3H_6O), [Co(NCMe)$_2$(L^4H_2)][$CoBr_4$]·5MeCN (**8**·5MeCN), [Co(NCMe)$_6$][$CoBr_3$(MeCN)]$_2$·2MeCN (**9**·2MeCN). For comparative structural/polymerisation studies, the complexes {CoBr(NCMe)L^5}$_2$·2MeCN (**10**·2MeCN) and [Co(NCMe)$_2L^5$]$_2$[$CoBr_3$(NCMe)]$_2$ (**11**), [FeBr(NCMe)L^5]$_2$·2MeCN (**12**·2MeCN) where L^5H = 2,6-$(CHO)_2$-4-*t*Bu-C_6H_2OH, as well as the chelate-free salt [Fe(NCMe)$_6$][$FeBr_3$OFeBr_3] (**13**) have been isolated and structurally characterized. The ability of these complexes to act as catalysts for the ring opening polymerisation (ROP) of ε-caprolactone (ε-CL) and δ-valerolactone (δ-VL) was investigated, as well as co-polymerisation of ε-CL with *rac*-lactide (*r*-LA) and *vice versa*.

Introduction

Global issues over plastic pollution continue to drive the search for alternative, more environmentally-friendly materials.[1] As part of our search for new catalysts capable of affording biodegradable polymers *via* the ring opening polymerisation (ROP) of cyclic esters, we have initiated investigations into the coordination chemistry of Schiff-base macrocycles derived from the [2 + 2] condensation of the dianilines [(X)(2-$C_6H_4NH_2)_2$] (X = CH_2CH_2, O) with the diformylphenols 2,6-$(CHO)_2$-4-R-C_6H_2OH (R = Me, *t*Bu) (Chart 1).[2] To date, we have reported how remote alkylaluminium centres bound to the macrocycle (X = CH_2CH_2) exhibited beneficial cooperative effects in the ROP of ε-caprolactone (ε-CL), whereas aluminoxane type (Al–O–Al) bonding proved to be detrimental.[3] Manganese complexes bearing these macrocycles were far less active (conversions <15%).[4] However, studies of mixed cobalt/zinc systems revealed interesting catalytic properties, with homo-dinuclear systems exhibiting inactivity while mixed-metal systems proved to be efficient for the ROP of ε-CL and δ-valerolactone (δ-VL).[5] It is also noteworthy that the structural chemistry of macrocycles of this type remains underexplored; a

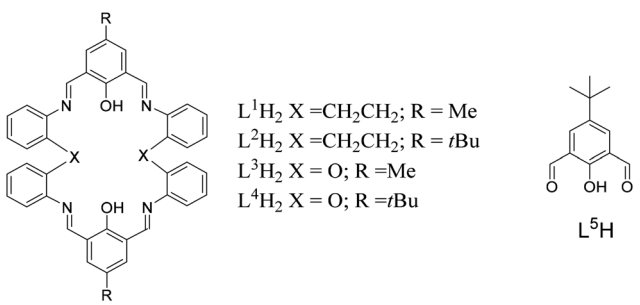

Chart 1 Synthesis of ligands L^1H_2–L^5H prepared herein.

[a]*Plastics Collaboratory, Department of Chemistry, University of Hull, HU6 7RX, UK. E-mail: c.redshaw@hull.ac.uk*
[b]*School of Chemistry, University of East Anglia, Norwich, NR4 7TJ, UK*

†Electronic supplementary information (ESI) available. CCDC 1849422, 2063728 and 2054028–2054038. For ESI and crystallographic data in CIF or other electronic format see DOI: 10.1039/d1dt00711d

search of the CSD revealed no hits,[6] other than our reported aluminium, manganese and cobalt systems.[3–5] Given this, we have re-focused our efforts on such Schiff-base systems and have extended our studies to iron, cobalt and copper complexes bearing [2 + 2] macrocycles derived from the dianilines $[(X)(2\text{-}C_6H_4NH_2)_2]$ (X = CH_2CH_2, O, Chart 2). Herein, we report the molecular structures of these complexes, and have screened a number of them for their capability in the ROP of ε-CL, δ-VL and *rac*-lactide (*r*-LA), and for the co-polymerisation of ε-CL with *r*-LA and *vice versa*. Poly(ε-caprolactone), PCL, and poly(lactide), PLA, are favoured polymers given their biodegradability properties, and their co-polymers are considered as potential environmentally-friendly commodity plastic.[7]

Results and discussion

–CH_2CH_2– bridged systems

Iron

Use R = Me L^1H_2. Iron is a cheap, earth abundant metal and its complexes have shown potential in the ROP of cyclic esters.[8] Given this, we have initiated studies on the iron chemistry of our [2 + 2] macrocyclic systems. The reaction of the macrocycle $\{[2\text{-}(OH)\text{-}5\text{-}Me\text{-}C_6H_2\text{-}1,3\text{-}(CH)_2][CH_2CH_2(2\text{-}C_6H_4N)_2]\}_2$ (L^1H_2) with two equivalents of $FeBr_2$ in refluxing toluene afforded, following work-up (MeCN), a brown crystalline solid in moderate yield. Single crystals were grown from a saturated solution of acetonitrile on standing at ambient

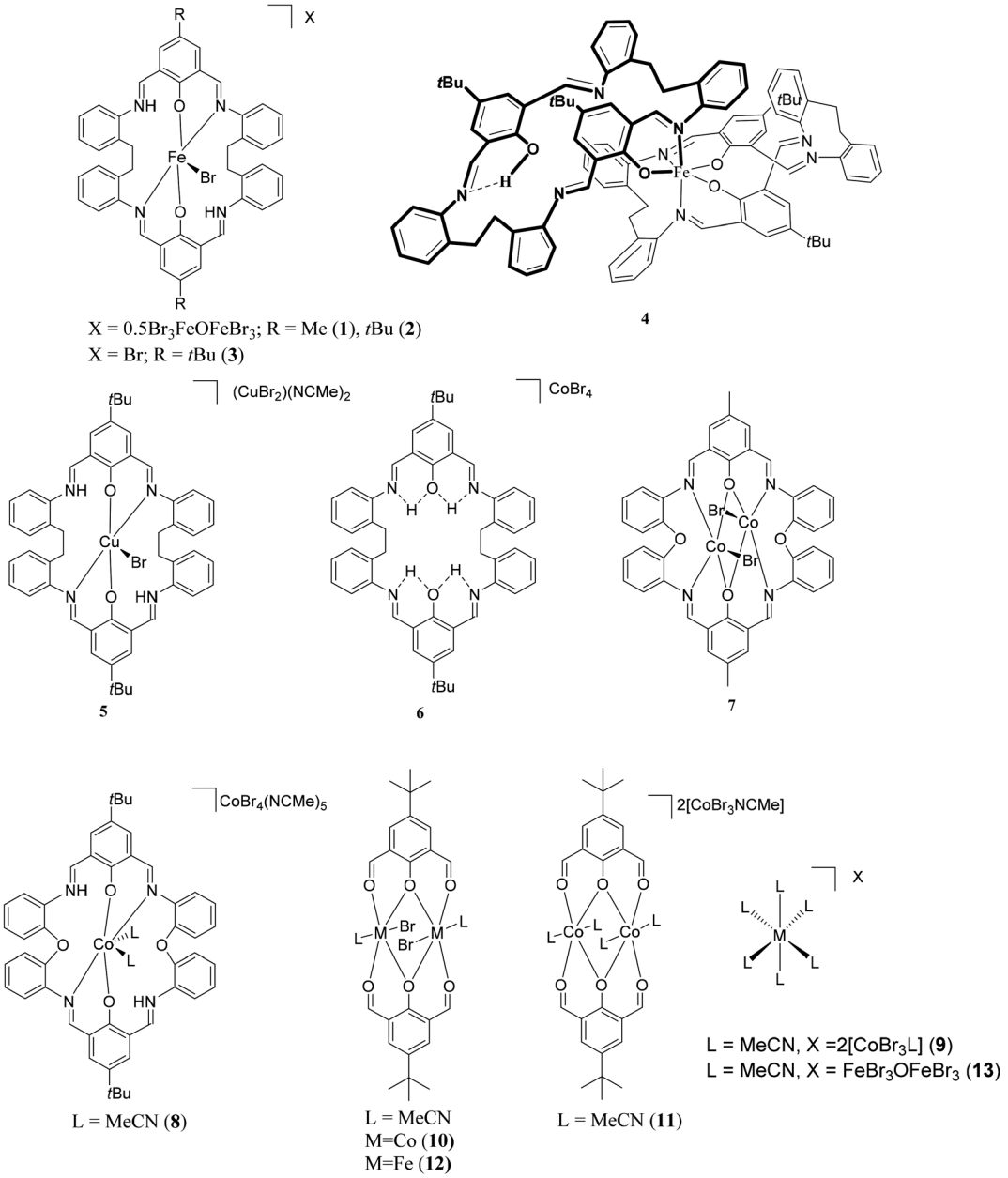

Chart 2 Structures of iron and cobalt complexes **1–13** prepared herein.

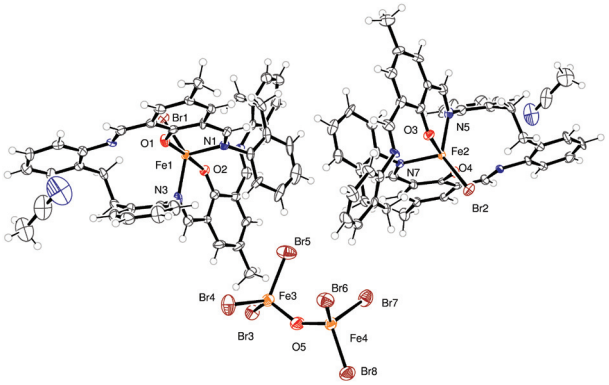

Fig. 1 Asymmetric unit for the structure of $[FeBr(L^1)]_2[Br_3FeOFeBr_3]\cdot 2(MeCN)$ (**1**·2MeCN). Thermal ellipsoids are drawn at the 50% probability level. Selected bond lengths (Å) and angles (°): Fe(1)–O(1) 2.002(6), Fe(1)–O(2) 2.020(6), Fe(1)–N(1) 2.129(7), Fe(1)–N(3) 2.138(7), Fe(1)–Br(1) 2.5070(16), Fe(2)–O(3) 2.031(6), Fe(2)–N(5) 2.150(7), Fe(2)–N(7) 2.135(7), Fe(2)–Br(2) 2.5104(15); O(1)–Fe(1)–O(2) 177.0(2), N(1)–Fe(1)–N(3) 103.8(3), Br(1)–Fe(1)–N(1) 120.26(19), N(5)–Fe(2)–N(7) 102.9(3).

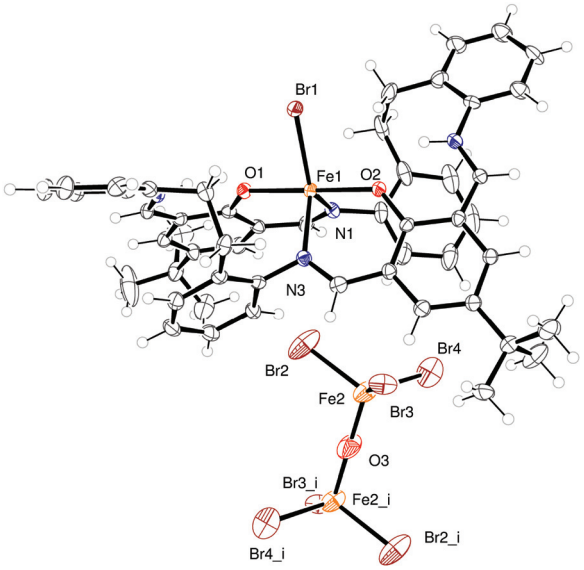

Fig. 2 View of the $[FeBr(L^2)][(FeBr_3)_2O]_{0.5}\cdot 0.5(MeCN)$ (**2**·0.5MeCN) complex ion, indicating the atom numbering scheme. Thermal ellipsoids are drawn at the 50% probability level. Symmetry equivalent atoms are generated by i = 1 − *x*, 1 − *y*, 1 − *z*. Selected bond lengths (Å) and angles (°): Fe(1)–O(1) 2.052(3), Fe(1)–O(2) 2.059(3), Fe(1)–N(1) 2.131(4), Fe(1)–N(3) 2.124(4), Fe(1)–Br(1) 2.4967(8); Br(1)–Fe(1)–O(1) 89.71(9), O(1)–Fe(1)–N(3) 94.83(14).

temperature for 3 days. The molecular structure is shown in Fig. 1, with selected bond lengths and angles given in the caption. There are two macrocyclic iron complexes in the asymmetric unit, related by a pseudosymmetric translation of *c*/2 (see ESI†), plus an anion of $[Br_3FeOFeBr_3]$ and two molecules of acetonitrile. Of the macrocyclic bound iron centres, both Fe1 and Fe2 adopt a distorted trigonal bipyramidal geometry (τ = 0.69),[9] bound by a bromide and two nitrogen atoms and two oxygen atoms of the macrocycle, apical sites are occupied by O atoms, with the bromide and N atoms in the equatorial sites. The composition is thus $[FeBr(L^1)]_2[Br_3FeOFeBr_3]\cdot 2(MeCN)$ (**1**·2MeCN). In terms of charge, the 2+ available from the anion which contains two Fe(III) centres, is balanced by the two cations (2× + 1), each of which contains an Fe(II) centre.

Use R = tBu L^2H_2. Similar reaction of $\{[2\text{-}(OH)\text{-}5\text{-}(t\text{Bu})\text{-}C_6H_2\text{-}1,3\text{-}(CH)_2][CH_2CH_2(2\text{-}C_6H_4N)_2]\}_2$ (L^2H_2) with 2.1 equivalents of $FeBr_2$ afforded, following work-up, red needles in good yield. Crystals suitable for X-ray diffraction were grown from a saturated solution of acetonitrile at ambient temperature. A view of the molecular structure is shown in Fig. 2, and bond lengths and angles are given in the caption. The crystal comprises $FeBr(L^2H_2)$ cations, $(FeBr_3)_2O$ anions and MeCN solvent molecules. The anions lie about a centre of symmetry and the solvent molecule sites refine best with half-occupancy; the molecular formula is therefore $[FeBr(L^2H_2)]$, $0.5[(FeBr_3)_2O]\cdot 0.5(MeCN)$ (**2**·0.5MeCN), and like **1**·2MeCN, is a mixed oxidation state Fe(II)/Fe(III) system. The iron atom in the cation is five-coordinate with a trigonal bipyramidal pattern (τ = 0.82);[9] the apical sites are occupied by O atoms, with the bromide and N atoms in the equatorial sites. There is a pseudo two-fold symmetry axis along the Fe–Br bond. In the macrocyclic ligand, there are four N atoms, each involved in a double bond, *viz.* C11═N2 1.298(5) C52═N1 1.287(6) C26═N3 1.296 (6) C37═N4 1.308 (7), N1 and N3 are coordinated to the Fe atom, while N2 and N4 are bonded to two C atoms (one with a double bond) and a hydrogen atom. The hydrogen atoms were included in the structure factor calculations in a planar, trigonal fashion, and their U_{iso} values were refined freely and satisfactorily; it is believed that both these groups are charged C–N^+H═C groups. Both these hydrogen atoms are involved in intramolecular hydrogen bonds.

The $(FeBr_3)_2O$ anion lies about a centre of symmetry. One of the bromide ligands is disordered over two sites, in an 82 : 18 occupancy ratio. The nearest neighbours of the bromide atoms are atoms of the disordered *t*-butyl group.

Similar treatment of $\{[2\text{-}(OH)\text{-}5\text{-}(t\text{Bu})\text{-}C_6H_2\text{-}1,3\text{-}(CH)_2][O(2\text{-}C_6H_4N)_2]\}_2$, but with limited $FeBr_2$ (1.1 equivalents), led to the isolation of the Fe(II) salt $[FeBr(L^2H_2)]Br\cdot 3MeCN$ (5.5MeCN). The molecular structure is provided in the ESI (Fig. S2†).

Use of [KFe(OtBu)$_3$(THF)]. Given alkoxide species play a central role in metal-catalysed ROP, we attempted to generate an iron alkoxide species. Reaction of L^2H_2 with *in situ* generated $[KFe(OtBu)_3(THF)]$ in refluxing toluene resulted, after work-up, in the isolation of a brown crystalline material. Crystals grown from a saturated solution of acetonitrile were found to be a bis-chelate structure $[Fe(L^2)(L^2H)]\cdot 3MeCN$ (**4**·3MeCN) (see Fig. 3), in which a distorted octahedral iron(III) centre is bound to two of the macrocyclic ligands. The asymmetric unit contains one iron complex and 3 molecules of acetonitrile. The coordination at the iron is such that one macrocycle is bound only in chelate fashion *via N,O*-type ligation, whilst the second macrocycle utilizes four atoms to bind in 2× *N,O*-type fashion. We have observed similar binding modes recently for aluminium.[3c]

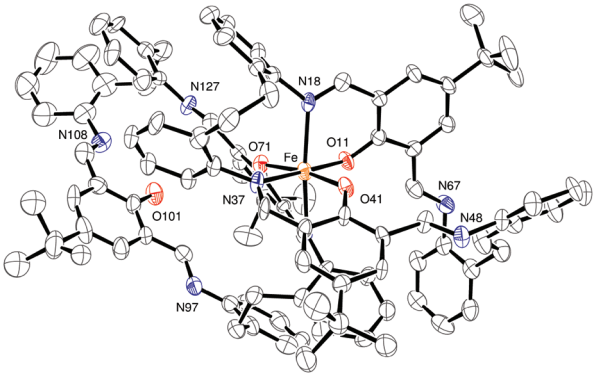

Fig. 3 View of $[Fe(L^2)(L^2H)]\cdot 3MeCN$ (**4**·3MeCN), indicating the atom numbering scheme. Thermal ellipsoids are drawn at the 50% probability level. For clarity hydrogen atoms are not shown. Selected bond lengths (Å) and angles (°): Fe(1)–O(11) 1.936(4), Fe–O(41) 1.931(4), Fe–O(71) 1.905(4), Fe–N(18) 2.234(5), Fe–N(37) 2.189(5), Fe–N(78) 2.240(5); O(11)–Fe–O(41) 92.1(2), O(11)–Fe–N(37) 176.6(2), N(18)–Fe–N(78) 164.0(2).

Use of copper bromide. Copper is also an earth abundant metal, though it has had only limited success in the ROP of cyclic esters.[10] For the successful systems, Schiff-base ligation appears beneficial, suggesting that interaction with the macrocyclic systems of the type herein could lead to a ROP active complex. Reaction of L^2H_2 with two equivalents of $CuBr_2$ afforded, following work-up, the orange/brown Cu salt complex $[CuBr(L^2H_2)][CuBr_2]\cdot 2MeCN$ (**5**·2MeCN) in good yield. In the cation, the copper centre is distorted trigonal bipyramidal with oxygens at the apex and two nitrogens and a bromide in the equatorial plane ($\tau = 0.90$).[9] The anion $Cu(I)Br_2^-$ resides close to a pocket formed by the macrocycle, see Fig. 4.

Attempted mixed-metal systems

Having successfully isolated mixed cobalt/zinc systems, which were active for ring opening polymerization whereas the analogous homodinuclear species were not,[5] we attempted to prepare mixed cobalt/titanium complexes. Our entry point was again the cobalt complex $[CoBrL^2H_2][CoBr_3(NCMe)]$, and reaction with $[TiCl_4]$ resulted in $[L^2H_4][CoBr_4]\cdot 2MeCN$ (**6**·2MeCN) as the only crystalline product. The molecular structure of the salt **6** comprises a protonated macrocycle L^2H_2 and the Co(II) containing anion $[CoBr_4]^{2-}$; see ESI (Fig. S4†) for details.

–O– bridged systems

We have also initiated a programme to investigate the coordination chemistry of the oxy-bridged macrocycles $\{[2\text{-}(OH)\text{-}5\text{-}(R)\text{-}C_6H_2\text{-}1,3\text{-}(CH)_2][O(2\text{-}C_6H_4N)_2]\}_2$ (R = Me L^3H_2, *t*Bu L^4H_2). Reaction of L^3H_2 with two equivalents of $CoBr_2$ afforded, following work-up (acetone), the complex $[(CoBr)_2L^3]\cdot 2C_3H_6O$ (**7**·$2C_3H_6O$), containing two Co(II) centres, as black crystals in *ca.* 40% isolated yield. Single crystals can be grown from a saturated solution of acetone at ambient temperature, and the molecular structure is shown in Fig. 5; selected bond lengths and angles are given in the caption. Both cobalt centres adopt distorted trigonal bipyramidal with a bromide at each apex (τ = 0.59 and 0.53 for Co1 and Co_2, respectively).[9]

In the case of L^4H_2, reaction with $CoBr_2$ afforded, following work-up (MeCN), two sets of crystals (~90 : 10). Both sets were subjected to single crystal X-ray diffraction, and the major product, as shown in Fig. 6, was found to be the Co(II) containing salt $[Co(NCMe)_2(L^4H_2)][CoBr_4]\cdot 5MeCN$ (**8**·5MeCN). In the cation, the cobalt centre is distorted octahedral, and is bound by two phenoxide oxygens and the two nitrogens N(1) and N(3) of the macrocycle plus two bound acetonitrile ligands. In the solid-state, there are C–H···Br interactions present. The minor product was found to be Co(II) containing salt [Co

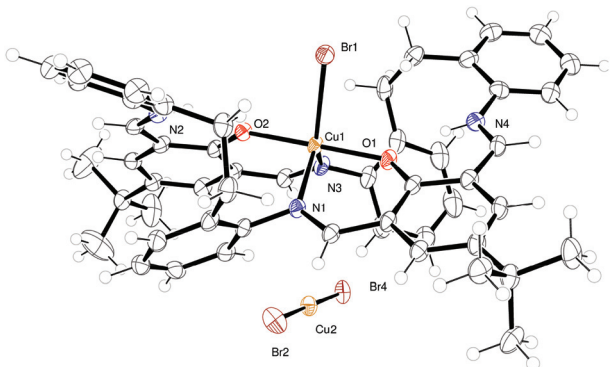

Fig. 4 Molecular structure of $[CuBr(L^2H_2)][CuBr_2]\cdot 2MeCN$ (**5**·2MeCN) with atoms drawn as 50% probability ellipsoids. Solvent molecules are not shown. Selected bond lengths (Å) and angles (°): Cu(1)–O(1) 1.955(3), Cu(1)–O(2) 1.948(3), Cu(1)–N(1) 2.106(3), Cu(1)–N(3) 2.074(3), Cu(1)–Br(1) 2.4790(6); O(1)–Cu(1)–O(2) 179.8(1), N(1)–Cu(1)–Br(1) 119.58(9), N(3)–Cu(1)–Br(1) 125.8(1).

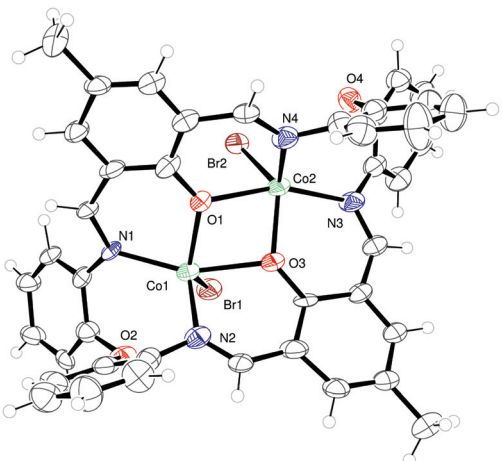

Fig. 5 Molecular structure of $[(CoBr)_2(L^3)]\cdot 2C_3H_6O$ (**7**·$2C_3H_6O$) with atoms drawn as 50% probability ellipsoids. Selected bond lengths (Å) and angles (°): Co(1)–O(1) 1.982(11), Co(1)–O(3) 2.216(11), Co(1)–N(1) 2.067(12), Co(1)–N(2) 2.091(13), Co(1)–Br(1) 2.421(3), Co(2)–O(1) 2.179(11), Co(2)–O(3) 1.977(11), Co(2)–N(3) 2.102(14), Co(2)–N(4) 2.079(13), Co(2)–Br(2) 2.421(3); O(1)–Co(1)–O(3) 70.0(4), N(1)–Co(1)–N(2) 112.3(5), O(1)–Co(1)–Br(1) 122.2(3), O(1)–Co(2)–N(3) 157.8(5), N(4)–Co(2)–Br(2) 111.2(4).

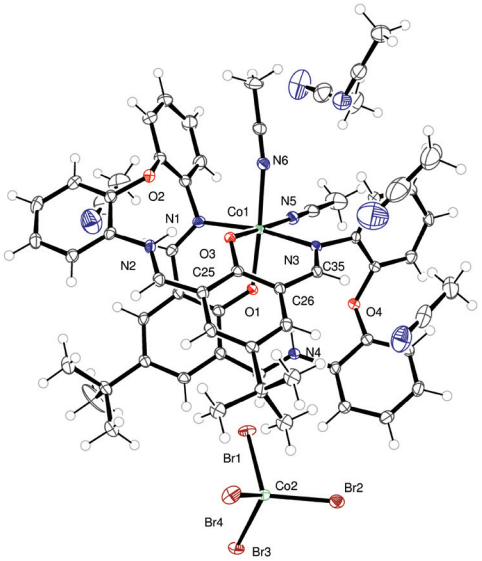

Fig. 6 Molecular structure of $[Co(NCMe)_2(L^4)][CoBr_4]\cdot 5MeCN$ (**8**·5MeCN) with atoms drawn as 50% probability ellipsoids. Selected bond lengths (Å) and angles (°): Co(1)–O(1) 2.016(3), Co(1)–O(3) 2.056(3), Co(1)–N(1) 2.156(3), Co(1)–N(3) 2.156(3), Co(1)–N(5) 2.121(3), Co(1)–N(6) 2.114(3); O(1)–Co(1)–O(3) 91.98(11), N(1)–Co(1)–N(3) 169.15(12), O(1)–Co(1)–N(6) 174.71(13), O(3)–Co(1)–N(5) 174.77(13)°.

$(NCMe)_6][CoBr_3NCMe]_2\cdot 2MeCN$ (**9**·2MeCN), details of this structure can be found in the ESI (Fig. S4†).

'Dialdehyde' systems

To probe the role played by the presence of the macrocycle during catalysis (see ROP section), we have also prepared cobalt complexes bearing chelate ligands derived from the 4-*tert*-butyl-2,6-diformylphenol 2,6-$(CHO)_2$-4-*t*Bu-C_6H_2OH (L^5H). Reaction of L^5H with $CoBr_2$ in the presence of excess Et_3N afforded, after work-up (MeCN), the Co(II) complex $\{[CoBr(NCMe)]L^5\}_2\cdot 2MeCN$ (**10**·2MeCN) as orange/brown prisms in good yield. The molecular structure is shown in Fig. 7, with selected bond lengths and angles given in the caption. Each cobalt centre is distorted octahedral, and are bound by oxygens from two L ligands and a bromide and acetonitrile ligand. The ligand arrangement is such that one bromide and an MeCN ligand reside above the Co_2O_6 plane and one bromide and an MeCN ligand are below this plane.

If the same reaction is conducted in the absence of Et_3N, then, following work-up (MeCN), green prisms are isolated in good yield. The molecular structure (see Fig. 8 for the cation) revealed the structure of the complex to be Co(II) containing salt $[Co(NCMe)_2L^5]_2[CoBr_3(NCMe)]_2$ (**11**). The dimer is centrosymmetric – the second half of the dimer is generated by the symmetry operation $-x, 1-y, 1-z$. Each cobalt centre in the cation is distorted octahedral, but unlike **10**, there is no bound bromide.

If a similar reaction is conducted with $FeBr_2$ in the presence of Et_3N, then, following work-up (MeCN), black prisms are isolated in good yield. The molecular structure (Fig. S5†) revealed the structure of the Fe(II) complex to be $[FeBr(NCMe)L^5]_2\cdot 2MeCN$ (**12**·2MeCN). Each iron centre in the cation is distorted octahedral, bound by oxygens from two L ligands, a bromide and an acetonitrile ligand.

Finally, for comparative catalytic studies, the salt $[Fe(NCMe)_6][FeBr_3OFeBr_3]$ (**13**) was prepared from L^1H_2 and $FeBr_3$.

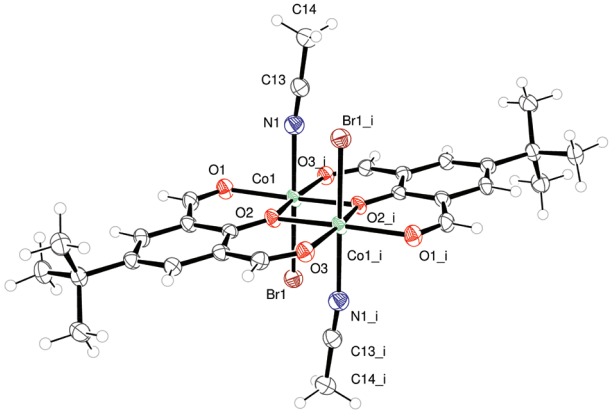

Fig. 7 Molecular structure of $\{[CoBr(NCMe)]L^5\}_2\cdot 2MeCN$ (**10**·2MeCN) with atoms drawn as 50% probability ellipsoids (unbound solvent not shown). Selected bond lengths (Å) and angles (°): Co(1)–O(1) 2.052(2), Co(1)–O(2) 2.079(2), Co(1)–Br(1) 2.5751(6), Co(1)–N(1) 2.163(3); O(1)–Co(1)–O(2) 87.17(8), Co(1)–O(2)–Co(1_i) 100.59(9), Br(1)–Co(1)–N(1) 169.51(8).

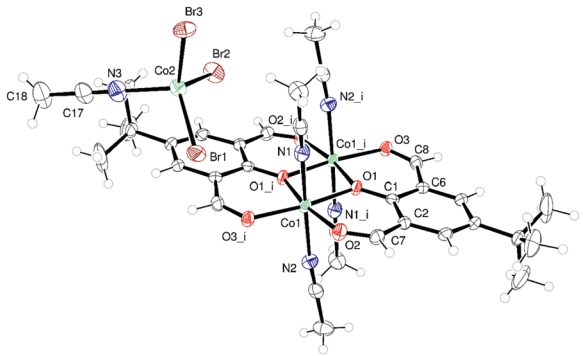

Fig. 8 Molecular structure of $[Co(NCMe)_2L^5]_2[CoBr_3(NCMe)]_2$ (**11**) with atoms drawn as 50% probability ellipsoids. Symmetry operation used to generate equivalent atoms: i = $-x, 1-y, 1-z$. Selected bond lengths (Å) and angles (°): Co(1)–O(1) 2.046(2), Co(1)–O(2) 2.050(2), Co(1)–N(1) 2.108(3), Co(1)–N(2) 2.143(3); O(1)–Co(1)–O(2) 88.56(9), Co(1)–O(2)–Co(1i) 99.59(9), N(1)–Co(1)–N(2) 172.07(11).

Ring opening polymerisation (ROP) of ε-CL and δ-VL

The Fe, Cu and Co complexes **1**, **2**, **4**, **5**, **9**–**13** have been screened for their ability to ring open polymerise ε-caprolactone (ε-CL) and δ-valerolactone (δ-VL); runs were conducted in the presence of benzyl alcohol (BnOH). For complexes **1**, **2** and **4**, a variety of conditions were used in the attempted ROP of ε-

Table 1 Synthesis of polycaprolactone using catalysts **1**, **2**, **4**, **9–13**

Run	Cat.	[Monomer] : [cat] : BnOH	T (°C)	t/h	Conv.[a] (%)	$M_n \times 10^3$ [b]	$M_{n_{Calcd}} \times 10^4$ [c]	PDI[d]
1	**1**	500 : 1 : 1	130	24	63.2	3.70	3.61	1.95
2	**1**	250 : 1 : 1	130	24	88.7	2.95	2.54	3.28
3	**1**	500 : 1 : 1	130	12	79.4	0.97	4.53	1.11
4	**1**	500 : 1 : 1	130	12	66.3	0.70	3.79	1.17
5	**2**	500 : 1 : 1	130	24	99.3	5.92	5.66	1.56
6	**2**	250 : 1 : 1	130	24	55.0	2.60	1.58	1.06
7	**4**	500 : 1 : 1	130	24	68.9	8.67	3.94	1.75
8	**4**	250 : 1 : 1	130	24	87.6	7.52	2.50	1.58
9	**9**	500 : 1 : 1	130	24	—	—	—	—
10	**10**	500 : 1 : 1	130	24	—	—	—	—
11	**11**	500 : 1 : 1	130	24	—	—	—	—
12	**12**	500 : 1 : 1	130	24	8.4	—	0.45	—
13	**13**	500 : 1 : 1	130	24	15.3	—	0.87	—

[a] Conversion was confirmed by ^{1}H NMR spectroscopy. [b] Determined by GPC analysis calibrated with polystyrene standards and multiplied by correction factor of 0.56. [c] F.W. ([M]/[BnOH])(conversion) + BnOH. [d] Polydispersity index (M_w/M_n) were determined by GPC.

CL including differing ratios of [ε-CL] : [Cat] : [BnOH] and run times, and it was found that the Fe compounds were far more active than the other metal complexes screened herein. ROP systems based on Fe,[8] Cu[10] and Co[5,11] have been reported with mixed success.

The polymerisation data for the ε-CL runs is given in Table 1. Highest conversion was achieved using **2** in run 5 using the ratio 500 : 1 : 1 at 130 °C over 24 h, albeit with less control than observed in run 6 using 250 : 1 : 1. Systems employing **1** and **4** were also less controlled, whilst the non-macrocyclic cobalt systems **9–11** proved to be inactive under the conditions employed herein. Interestingly, the non-macrocyclic iron complexes **12** and **13** proved to be poorly active with low conversions for ε-CL. However, for δ-VL, a 32% conversion (affording small molecular weight oligomers) was observed for **13**, whereas **12** was inactive. The MALDI-TOF spectra can be interpreted using the formula C_6H_6–$CH_2O[O(CH_2)_5CO]_nOH$, for example see run 5 (Fig. S7, ESI†). The ^{1}H NMR spectrum of the PCL indicated the presence of benzyloxy and hydroxyl end groups (Fig. S8, ESI†). There was evidence of significant transesterication, whilst all observed M_n values were significantly lower than the calculated values.

In the case of δ-VL (Table 2), complexes **1** and **2** exhibited better conversions *versus* **4** and **12**, whilst **5**, **9**, **10** and **11** proved to be inactive. In the MALDI-TOF mass spectra of the PVL, a number of families of peaks were observed separated by 100 mass units (Fig. S22, ESI†) can be assigned by the formula C_6H_6–$CH_2O[O(CH_2)_4CO]_nOH$; the highest were typically about 6000 (run 4, Fig. S21†). The ^{1}H NMR spectra of the PVL (*e.g.* Fig. S20†) revealed the presence of benzyloxy and OH end groups. The observed molecular weights were lower than the calculated values, suggesting the presence of a chain transfer agent (H_2O or BnOH).

From a kinetic study (Fig. S11 and S18†), it was observed that the polymerisation rate exhibited near first order dependence on the ε-CL or δ-VL concentration at 130 °C, and complex **2** displayed the best rate in both δ-VL [K_{obs} = 7.29 × 10^{-3} h^{-1}] and ε-CL polymerisations [K_{obs} = 4.70 × 10^{-3} h^{-1}].

Table 2 ROP of δ-VL using complexes **1**, **2**, **4**, **5**, **9–13**

Run	Cat.	[VL] : [Cat] : BnOH	T (°C)	t/h	Conv.[a] (%)	$M_n \times 10^3$ [b]	$M_{n_{Calcd}} \times 10^4$ [c]	PDI[d]
1	**1**	500 : 1 : 1	130	24	98.6	2.52	4.94	1.14
2	**1**	250 : 1 : 1	130	24	94.3	3.10	2.36	1.28
3	**1**	500 : 1 : 1	130	12	39.7	—	2.00	—
4	**2**	500 : 1 : 1	130	24	96.1	6.00	4.92	1.38
5	**2**	250 : 1 : 1	130	24	93.2	4.53	2.41	1.23
6	**2**	500 : 1 : 1	130	12	83.8	—	4.20	—
7	**4**	500 : 1 : 1	130	24	34.5	2.59	1.84	1.25
8	**4**	250 : 1 : 1	130	24	23.5	2.51	0.60	1.27
9	**5**	500 : 1 : 1	130	24	—	—	—	—
10	**9**	500 : 1 : 1	130	24	—	—	—	—
11	**10**	500 : 1 : 1	130	24	—	—	—	—
12	**11**	500 : 1 : 1	130	24	—	—	—	—
13	**12**	500 : 1 : 1	130	24	—	—	—	—
14	**13**	500 : 1 : 1	130	24	32.0	0.76	2.18	1.26

[a] Conversion was confirmed by ^{1}H NMR spectroscopy. [b] Determined by GPC analysis calibrated with polystyrene standards and multiplied by correction factor of 0.58. [c] F.W. ([M]/[BnOH])(conversion) + BnOH. [d] Polydispersity index (M_w/M_n) were determined by GPC.

Table 3 Synthesis of block copolymers from cyclic ester monomers using the Fe catalysts **1**, **2** and **4**

Run	Composition	Catalyst	t (h)	Incorporated amount[a]	$M_n \times 10^{3}$ [b]	PDI
1	Poly (ε-CL + *r*-LA) [ε-CL] : [*r*-LA] : [cat] : [BnOH] = 500 : 500 : 1 : 1	**1**	24 + 24 :	ε-CL : *r*-LA = 47 : 53	3.75	2.22
2	Poly (δ-VL + *r*-LA) [δ-VL] : [*r*-LA] : [cat] : [BnOH] = 500 : 500 : 1 : 1	**1**	24 + 24	δ-VL : *r*-LA = 14 : 86	5.51	1.73
3	Poly (*r*-LA + ε-CL) [*r*-LA] : [ε-CL] : [cat] : [BnOH] = 500 : 500 : 1 : 1	**2**	24 + 24	*r*-LA : ε-CL = 49 : 51	10.55	1.51
4	Poly (*r*-LA + ε-CL) [ε-CL] : [*r*-LA] : [cat] : [BnOH] = 250 : 250 : 1 : 1	**2**	24 + 24	*r*-LA : ε-CL = 93 : 7	6.20	1.82
5	Poly (ε-CL + *r*-LA) [ε-CL] : [*r*-LA] : [cat] : [BnOH] = 500 : 500 : 1 : 1	**2**	24 + 24	ε-CL : *r*-LA = 60 : 40	9.31	1.64
6	Poly (ε-CL + *r*-LA) [ε-CL] : [*r*-LA] : [cat] : [BnOH] = 250 : 250 : 1 : 1	**2**	24 + 24	ε-CL : *r*-LA = 63 : 37	12.63	3.02
7	Poly (δ-VL + *r*-LA) [δ-VL] : [*r*-LA] : [cat] : [BnOH] = 500 : 500 : 1 : 1	**2**	24 + 24	δ-VL : *r*-LA = 55 : 45	3.40	1.26
8	Poly (δ-VL + *r*-LA) [δ-VL] : [*r*-LA] : [cat] : [BnOH] = 250 : 250 : 1 : 1	**2**	24 + 24	δ-VL : *r*-LA = 88 : 12	2.57	2.56
9	Poly (ε-CL + *r*-LA) [ε-CL] : [*r*-LA] : [cat] : [BnOH] = 500 : 500 : 1 : 1	**4**	24 + 24	ε-CL : *r*-LA = 100 : 0	4.61	1.23
10	Poly (ε-CL + *r*-LA) [ε-CL] : [*r*-LA] : [cat] : [BnOH] = 250 : 250 : 1 : 1	**4**	24 + 24	ε-CL : *r*-LA = 90 : 10	3.61	1.18

[a] Conversion was confirmed by ^{1}H NMR spectroscopy. [b] Determined by GPC analysis calibrated with polystyrene standards and multiplied by correction factor of 0.56.

Synthesis of block co-polymers

The co-polymerisation of ε-CL with *r*-LA and of δ-VL with *r*-LA was also examined (Table 3). Noteworthy, the co-polymerisation of ε-CL with *r*-LA is much easier than δ-VL with *r*-LA when using the Fe complexes. In the presence of complex **2**, the M_n of the block co-poly(ε-CL + *r*-LA) reached around 12 000. Complexes **1** and **4** were less active in these co-polymerisations. As observed by ^{1}H NMR spectroscopy (Fig. S14 and S24†), the co-polymers were also capped by benzyloxy and hydroxyl end groups. The composition of the copolymer was further illustrated by ^{13}C NMR spectroscopy (Fig. S17 and S25†). From the MALDI-ToF mass spectrum (positive mode) of poly(ε-CL + *r*-LA) a gap of 114 corresponding to the molecular weight of ε-CL was evident, whilst running the spectra in negative method revealed a gap of 144 corresponding to the molecular weight of *r*-LA (Fig. S12 and 13†). The MALDI-ToF mass spectrum for co-poly (δ-VL + *r*-LA) was also recorded, see Fig. S26.† The 2D J-resolved ^{1}H NMR spectrum for the copolymer was recorded and the peaks were assigned to the corresponding tetrads (see Fig. S17 and S22, ESI†) according to literature reports,[12] which revealed an atactic LA–LA–LA chain.

Conclusion

In conclusion, we have successfully synthesised iron, cobalt and copper complexes bearing [2 + 2] Schiff-base macrocycles derived from dianilines containing CH_2CH_2 bridges. Cobalt complexes were prepared from a related dianiline containing an oxy bridge. A number on non-macrocyclic Fe and Co complexes were also prepared for comparative catalytic studies. The iron complexes outperformed the other metal systems herein for the ring opening polymerisation of both ε-caprolactone and δ-valerolactone. Best results were obtained using the iron salt **2**, however the non-macrocyclic system **12** also performed well. Complex **2** was also capable of the copolymerisation of ε-CL (or δ-VL) with *rac*-lactide, affording copolymers appreciable amounts of each monomer incorporated.

Experimental

General

All manipulations were carried out under an atmosphere of nitrogen using standard Schlenk and cannula techniques or in a conventional nitrogen-filled glove-box. Toluene was refluxed over sodium, whilst acetonitrile was refluxed over calcium hydride. IR spectra (nujol mulls, KBr windows) were recorded on a Nicolet Avatar 360 FT-IR spectrometer; ^{1}H and ^{13}C NMR spectra were recorded at room temperature on a Varian VXR 400 S spectrometer at 400 MHz or a Gemini 300 NMR spectrometer or a Bruker Advance DPX-300 spectrometer. The ^{1}H NMR spectra were calibrated against the residual protio impurity of the deuterated solvent. Elemental analyses were performed by the elemental analysis service at the London Metropolitan University, the Chemistry Department at the University of Hull or Nanjing University. The precursors 2,6-$(CHO)_2$-4-R-C_6H_2OH (R = Me, *t*Bu) and 2,2′-ethylenedianiline (or 2,2′-oxydianiline) and the Schiff-base pro-ligands were prepared by the literature.[3a,c,13–15] For the iron and cobalt complexes, all manipulations were carried out under an atmosphere of dry nitrogen using conventional Schlenk and cannula techniques or in a conventional nitrogen-filled glove box. All solvents were distilled and degassed prior to use (Table 2).

Synthesis of $[FeBr(L^1H_2)]_2[(FeBr_3)_2O]\cdot 2(MeCN)$ (1·2MeCN)

L^1H_2 (0.52 g, 0.77 mmol) and $FeBr_2$ (0.34 g, 1.58 mmol) were combined in a Schlenk and toluene (20 mL) was added. After refluxing for 12 h, the volatiles were removed *in-vacuo*, and the residue was extracted into MeCN (20 mL). Prolonged standing at room temperature afforded orange/brown prisms. Yield: 0.72 g, 78%. Elemental analysis calculated for $C_{96}H_{82}Br_8Fe_4N_{10}O_5$: required: C 49.32% H 3.60% N 5.00% Found: 49.88% H 3.58% N 5.09%. IR (KBr, cm^{-1}): 3378 (s), 2923 (s), 2726 (w), 2671 (w), 2360 (w), 1633 (m), 1585 (m), 1538 (m), 1462 (s), 1377 (s), 1300 (w), 1280 (w), 1238 (m), 1102 (m), 977 (w), 873 (w), 801 (m), 754 (m), 722 (m), 688 (w), 622 (w), 574 (w), 534 (w), 502 (m), 486 (w), 455 (w). M.S. (MALDI-ToF): 817 (M^+). Magnetic moment: 6.35 B.M.[16]

Synthesis of $[FeBr(L^2H_2)]_2[(FeBr_3)_2O]\cdot 0.5MeCN$ (2·0.5MeCN)

To the pro-ligand L^2H_2 (0.50 g, 0.65 mmol) in toluene was added 2.1 equivalents of $FeBr_2$ (0.30 g, 1.39 mmol), and the system was refluxed for 12 h. On cooling, the volatiles were removed under vacuum, and the residue was extracted into acetonitrile (30 ml) to afford **2**·MeCN as red needles (0.48 g, 56%). Elemental analysis calculated for $C_{106}H_{107}Br_8Fe_4N_9O_5$: C 51.97, H 4.40, N 5.15%; found: C 51.21, H 4.43, N 5.55%. IR (KBr, cm^{-1}): 3168 (m), 2925 (s), 2854 (s), 2726 (w), 1704 (m), 1620 (m), 1587 (m), 1542 (s), 1462 (s), 1377 (s), 1317 (w), 1260 (w), 1233 (m), 1214 (m), 1180 (m), 1130 (w), 933 (w), 890 (w), 839 (w), 799 (m), 744 (m), 722 (m), 526 (m), 449 (m). M.S. (MALDI-ToF): 901 (M − anion). Magnetic moment: 5.86 B.M.[16]

Synthesis of $[FeBr(L^2H_2)]Br\cdot 3MeCN$ (5.5MeCN)

As for **2**, but using L^2H_2 (0.52 g, 0.68 mmol) and $FeBr_2$ (0.16 g, 0.74 mmol) affording **3**·5.5MeCN as brown prisms. Yield: 0.52 g, 65%. IR (KBr, cm^{-1}): 3168 (m), 2925 (s), 2854 (s), 2726 (w), 1636 (s), 1619 (s), 1599 (m), 1587 (m), 1537 (s), 1463 (s), 1377 (s), 1333 (m), 1283 (w), 1241 (m), 1183 (m), 1101 (m), 1063 (s), 1007 (m), 976 (m), 880 (s), 794 (m), 753 (s), 722 (m), 689 (m), 622 (w), 595 (w), 575 (w), 535 (w), 513 (m), 494 (m), 476 (w). M.S. (MALDI-ToF): 901 (M − 5.5MeCN − anion).

Synthesis of $[Fe(L^2)(L^2H)]\cdot 3MeCN$ (4·3MeCN)

To $FeBr_2$ (1.00 g, 4.64 mmol) was added KO*t*Bu (1.04 g, 9.27 mmol) in THF (30 ml) at 0 °C and the system was stirred for 5 h. Following removal of the volatiles, L^2H_2 (3.57 g, 4.64 mmol) and toluene (20 ml) was added and the system was refluxed for 12 h. On cooling, the volatiles were removed and the residue was extracted into cold acetonitrile (30 ml). **4**·3MeCN formed. Yield 1.62 g, 41%. Elemental analysis calculated for $C_{104}H_{101}FeN_8O_4$ (sample dried *in-vacuo* for 2 h): C 78.92, H 6.43, N 7.08%. Found C 79.09, H, 6.49, N On prolonged standing at ambient dark brown block. Yield: 1.84 g, 46.6%. IR (KBr, cm^{-1}): 3377 (w), 2958 (s), 2924 (s), 2854 (s), 2726 (w), 1630 (m), 1587 (m), 1461 (s), 1415 (w), 1377 (s), 1260 (s), 1202 (w), 1093 (s), 1019 (s), 863 (m), 800 (s), 755 (w), 740 (w), 723 (m), 705 (w), 662 (w), 566 (w), 530 (w), 504 (w), 465 (w). MS (Maldi): 1584 $(M + H)^+$. Magnetic moment: 5.07 B.M.[16]

Synthesis of $[CuBr(L^2H_2)][CuBr_2]\cdot 2MeCN$ (5·2MeCN)

As for **1**, but using L^2H_2 (0.52 g, 0.68 mmol) and $CuBr_2$ (0.30 g, 1.34 mmol), affording **5** as brown prisms. Yield 0.69 g, 84%. Elemental analysis calculated for $C_{52}H_{52}Br_3Cu_2N_4O_2$: C 55.18, H 4.63, N 4.95%. Found C 54.59, H, 4.48, N 4.93%. IR (KBr, cm^{-1}): 3171 (m), 2922 (s), 2853 (s), 2727 (s), 2671 (w), 2350 (w), 1633 (s), 1618 (s), 1594 (s), 1538 (s), 1463 (s), 1377 (s), 1336 (w), 1285 (m), 1260 (w), 1249 (m), 1239 (w), 1183 (m), 1156 (w), 1103 (m), 1062 (m), 1022 (w), 977 (w), 950 (w), 938 (w), 876 (s), 846 (m), 830 (m), 794 (m), 754 (s), 738 (w), 722 (s), 688 (m), 623 (m), 594 (w), 575 (m), 558 (m), 550 (m). M.S. (ESI): 908 (M − anion), 827 (M − anion − Br). Magnetic moment: 1.19 B.M.[17]

Synthesis of $[L^2H_4][CoBr_4]\cdot 2MeCN$ (6·2MeCN)

To $[CoBrL^2][CoBr_3(NCMe)]$ (1.00 g, 0.80 mmol) in toluene (30 mL) was added $[TiCl_4]$ (0.80 mL, 1.0 M, 0.80 mmol) and the system was refluxed for 12 h. On cooling, the volatiles were removed and the residue was extracted into acetonitrile (30 ml). On prolonged standing at 0 °C small red blocks of **6**·2MeCN formed. Yield: 0.38 g, 83%. Elemental analysis calculated for $C_{52}H_{54}Br_4CoN_4O_2$: C 54.52, H 4.75, N 4.89%. Found C 53.34, H, 5.19, N 4.95%. IR (KBr, cm^{-1}): 3381 (m), 2925 (s), 2924 (s), 2854 (s), 2726 (w), 2359 (w), 1636 (w), 1618 (s), 1594 (m), 1574 (w), 1538 (s), 1462 (s), 1377 (s), 1333 (s), 1285 (m), 1260 (m), 1183 (s), 1102 (m), 1063 (m), 1021 (m), 873 (m), 799 (s), 756 (m), 722 (m), 688 (w), 668 (w), 624 (w), 576 (w), 558 (w), 522 (w). M.S. (ESI): 847 (M − $CoBr_3$). 829 (M − Br_4). 766.97 (M − $CoBr_4$). Magnetic moment: 5.05 B.M.[18]

Synthesis of $[(CoBr)_2(L^3)]\cdot 2C_3H_6O$ (7·2C_3H_6O)

To the pro-ligand L^3H_2 (1.00 g, 1.52 mmol) in toluene was added 2.1 equivalents of $CoBr_2$ (0.70 g, 3.20 mmol), and the system was refluxed for 12 h. On cooling, the volatile were removed under vacuum, and the residue was extracted into acetone (30 ml) to afford **7**·2C_3H_6O as black crystals (0.98 g, 62%). Single crystals can also be grown from a saturated acetone solution of **7**. Elemental analysis calculated for $C_{42}H_{30}Br_2Co_2N_4O_4$: C 54.10, H 3.24, N 6.01%. Found C 53.88, H 3.19, N 6.25%. IR (KBr, cm^{-1}): 2924 (s), 2853 (s), 2727 (w), 1746 (w), 1693 (w), 1620 (m), 1587 (m), 1537 (m), 1463 (s), 1377 (s), 1261 (m), 1235 (m), 1215 (m), 1151 (w), 1106 (w), 1072 (m), 1030 (w), 891 (w), 867 (w), 842 (w), 800 (m), 757 (w), 722 (m), 534 (w), 478 (w), 449 (w). M.S. (ESI): 851 (M − 2C_3H_6O − Br), 714 (M − 2C_3H_6O − CoBr). Magnetic moment: 6.10 B.M.[18]

Synthesis of $[Co(NCMe)_2(L^4H_2)]\cdot[CoBr_4]$ 5MeCN (8·5MeCN)

To the pro-ligand L^4H_2 (1.00 g, 1.36 mmol) in toluene was added 2.1 equivalents of $CoBr_2$ (0.62 g, 2.83 mmol), and the system was refluxed for 12 h. On cooling, the volatile were removed under vacuum, and the residue was extracted into acetonitrile (30 ml) to afford **8**·3MeCN as red crystals, yield 0.86 g, 44%, and a smaller amount of green crystals of **9**, yield *ca*. 5%. Elemental analysis calculated for $C_{62}H_{65}Br_4Co_2N_{11}O_4$: C 49.55, H 4.00, N 6.67% Found for **8** C, 49.35, H 3.96, N 6.61%. IR (KBr, cm^{-1}): 3172 (m), 2956 (s), 2923 (s), 2853 (s),

2726 (w), 1619 (m), 1595 (m), 1536 (m), 1461 (s), 1377 (s), 1260 (s), 1155 (w), 1096 (s), 1060 (s), 1022 (s), 892 (w), 874 (w), 800 (s), 722 (s). M.S. (ESI): 933 (M − 7MeCN − 3Br), 817 (M − 7MeCN − 3Br − 2Co). Magnetic moment: 6.94 B.M.[18]

IR (KBr, cm^{-1}) for Complex **9**: 2922 (s), 2854 (s), 2727 (w), 2308 (m), 2282 (m), 2247 (m), 1658 (s), 1635 (s), 1580 (w), 1531 (s), 1464 (s), 1416 (s), 1377 (s), 1367 (s), 1354 (s), 1327 (w), 1287 (m), 1255 (m), 1244 (w), 1222 (m), 1149 (w), 1130 (w), 1098 (w), 1040 (m), 1014 (s), 930 (w), 917 (w), 846 (s), 801 (m), 772 (m), 757 (m), 727 (s), 627 (w), 550 (s), 531 (m), 430 (m).

Synthesis of {CoBr(NCMe)L^5}$_2$·2MeCN (10·2MeCN)

To L^5H (1.00 g, 4.85 mmol) and [$CoBr_2$] (1.05 g, 4.85 mmol) was added toluene (20 mL) and Et_3N (0.3 ml, 0.22 mmol) and the system was refluxed for 12 h. Following removal of volatiles *in-vacuo*, the residue was extracted into MeCN (20 mL), and on standing at ambient temperature large orange/brown prisms of **10**·3MeCN formed. Isolated yield: 1.41 g, 68%. Elemental analysis calculated for $C_{32}H_{38}Br_2Co_2N_4O_6$ (sample dried *in-vacuo* for 2 h): C 43.66, H 4.19, N 3.64. Found C 43.81, H 4.23, N 3.67%. IR (KBr, cm^{-1}): 2957 (s), 2924 (s), 2360 (s), 2342 (m), 2312 (m), 2284 (s), 1696 (m), 1641 (s), 1566 (m), 1535 (s), 1464 (s), 1402 (w), 1377 (s), 1367 (s), 1352 (w), 1259 (s), 1225 (m), 1093 (s), 1038 (s), 939 (m), 911 (m), 867 (w), 845 (m), 800 (s), 768 (s), 729 (s), 668 (m), 620 (m), 556 (s), 532 (m), 435 (m). M.S. (ESI): 733 (M − MeCN), 585 (M − 3MeCN − Co), 573 (M − MeCN − 2Br). Magnetic moment: 6.35 B.M.[18]

Synthesis of [Co(NCMe)$_2$$L^5$]$_2$[$CoBr_3$(NCMe)]$_2$ (11)

To L^5H (1.00 g, 4.85 mmol) and [$CoBr_2$] (1.05 g, 4.85 mmol) was added toluene (20 mL) and the system was refluxed for 12 h. Following removal of volatiles *in-vacuo*, the residue was extracted into MeCN (20 mL), and on standing at ambient temperature large green prisms of **11** formed. Isolated yield: 1.53 g, 46%. Elemental analysis calculated for $C_{36}H_{44}Co_4N_6O_6$ (sample dried *in-vacuo* for 2 h): C 47.43, H 4.73, N 6.91%. Found C 47.82, H 4.79, N 6.98%. IR (KBr, cm^{-1}): 2926 (s), 2854 (s), 2360 (m), 2342 (w), 2312 (s), 2284 (m), 1641 (s), 1621 (s), 1566 (m), 1535 (s), 1464 (s), 1402 (w), 1377 (s), 1367 (s), 1352 (w), 1259 (s), 1225 (m), 1093 (s), 1038 (s), 1019 (s), 845 (s), 800 (s), 768 (m), 758 (m), 729 (s), 668 (m), 620 (m), 556 (s), 532 (s), 435 (s). M.S. (ESI): 412 (M − 4MeCN − 2Co). Magnetic moment: 6.69 B.M.[18]

Synthesis of [FeBr(NCMe)L^5]$_2$·2MeCN (12·2MeCN)

To L^5H (1.00 g, 4.85 mmol) and [$FeBr_2$] (1.06 g, 4.85 mmol) was added toluene (20 mL) and Et_3N (0.7 ml, 0.485 mmol) and the system was refluxed for 12 h. Following removal of volatiles *in-vacuo*, the residue was extracted into MeCN (20 mL), and on standing at ambient temperature large orange/brown prisms of **10**·3MeCN formed. Isolated yield: 0.837 g, 40%. Elemental analysis calculated for $C_{28}H_{32}Br_2Fe_2N_2O_6$ (sample dried *in-vacuo* for 2 h): C 44.02, H 4.22, N 3.67. Found C 44.61, H 4.52, N 3.72%. IR (KBr, cm^{-1}): 3352 (w), 2954 (s), 2923 (s), 2854 (s), 2727 (w), 2360 (w), 2341 (w), 1643 (m), 1620 (m), 1528 (m), 1462 (s), 1377 (s), 1259 (m), 1160 (m), 1037 (s), 1016 (m), 842 (w), 800 (s), 769 (w), 755 (w), 722 (m), 668 (w), 618 (m), 539 (m). M.S. (ESI): 519 (M − 4MeCN − 2Br). Magnetic moment: 6.70 B.M.[18]

Synthesis of [Fe(NCMe)$_6$][$FeOBr_3$]$_2$ (13)

L^1H_2 (0.52 g, 0.77 mmol) and [$FeBr_3$] (0.47 g, 1.58 mmol) were combined in a Schlenk and toluene (20 mL) was added. After refluxing for 12 h, the volatiles were removed *in-vacuo*, and the residue was extracted into MeCN (20 mL). Prolonged standing at room temperature afforded brown prisms; isolated yield 0.39 g 81%. Elemental analysis calculated for $C_{12}H_{18}Br_6Fe_3N_6O$ (sample dried *in-vacuo* for 2 h): C 15.85, H 2.00, N 9.24%. Found C, 15.61 H, 2.12 N 9.31%. IR (KBr, cm^{-1}): 2925 (s), 2854 (s), 2361 (s), 2339 (s), 1868 (s), 1844 (s), 1830 (m), 1792 (m), 1772 (w), 1750 (m), 1734 (m), 1717 (m), 1700 (m), 1684 (m), 1669 (m), 1653 (m), 1646 (m), 1635 (m), 1616 (s), 1576 (s), 1559 (s), 1540 (s), 1521 (s), 1506 (s), 1497 (m), 1489 (m), 1457 (s), 1419 (m), 1377 (s), 1260 (s), 1089 (s), 800 (s), 668 (s).

ROP procedure

ε-Caprolactone and δ-valerolactone. Typical polymerisation procedure in the presence of one equivalent of benzyl alcohol (Table 1, run 1) is as follows. A toluene solution of **1** (0.010 mmol, in 1.0 mL toluene) and BnOH (0.010 mmol) were added into a Schlenk tube in the glove-box at room temperature. The solution was stirred for 2 min, and then ε-caprolactone (2.5 mmol) or δ-valerolactone along with 1.5 mL toluene was added to the solution. The reaction mixture was then placed into an oil bath pre-heated to the required temperature, and the solution was stirred for the prescribed time. The polymerisation mixture was then quenched by addition of an excess of glacial acetic acid (0.2 mL) into the solution, and the resultant solution was then poured into cold methanol (200 mL). The resultant polymer was then collected on filter paper and was dried *in vacuo*.

Co-polymerisations

A toluene solution of catalyst (0.010 mmol, in 1.0 mL toluene) was added into a Schlenk tube in the glove-box at room temperature. The solution was stirred for 2 min, and then 1 equivalent of BnOH (from 1 mmol BnOH in 100 ml toluene) and monomer were added, after 24 h the other monomer was added to the solution. The reaction mixture was then placed into an oil bath pre-heated to the 130 °C, and the solution was stirred for another 24 h. The polymerisation mixture was then quenched by addition of an excess of glacial acetic acid (0.2 mL) into the solution, and the resultant solution was then poured into cold methanol (200 mL). The resultant polymer was then collected on filter paper and was dried *in vacuo*.

Kinetic studies

The polymerisations were carried out at 130 °C in toluene (1 mL) using 0.010 mmol of complex. The molar ratio of monomer to initiator was fixed at 500 : 1, and at appropriate time intervals, 0.5 μL aliquots were removed (under N_2) and

Table 4 Crystallographic data

Compound	**1**·2MeCN	**2**·0.5MeCN	**3**·5.5MeCN	**4**·3MeCN
Formula	$C_{96}H_{86}Br_8Fe_4N_{10}O_5$	$C_{52}H_{52}BrFeN_4O_2$, C_2H_3N, 0.5(Br_6Fe_2O)	$C_{52}H_{52}BrFeN_4O_2$, Br, 5.5(C_2H_3N)	$C_{104}H_{101}FeN_8O_4$, (3MeCN)
Formula weight	2322.42	1224.841185.89	1185.89	1705.9
Crystal system	Monoclinic	Triclinic	Monoclinic	Monoclinic
Space group	$P2_1/n$	$P\bar{1}$	$P2_1/n$	$P2_1/c$
Unit cell dimensions				
a (Å)	15.6606(4)	13.6454(5)	14.2077(6)	12.6268(5)
b (Å)	16.0326(4)	13.9070(7)	27.6241(9)	30.3249(10)
c (Å)	37.4062(11)	15.6432(8)	15.1579(8)	24.6577(10)
α (°)	90	67.263(5)	90	90
β (°)	99.896(3)	88.642(4)	112.484(6)	100.817(3)
γ (°)	90	81.638(4)	90	90
V (Å^3)	9252.2(4)	2707.0(2)	5496.9(5)	9273.8(6)
Z	4	1	4	4
Temperature (K)	100(2)	100(2)	100(2)	140(1)
Wavelength (Å)	1.54184	0.71075	0.71073	0.71073
Calculated density (g cm^{-3})	1.667	1.503	1.185	1.222
Absorption coefficient (mm^{-1})	9.439	3.531	1.766	0.223
T_{min}, T_{max}	0.755, 1.000	0.592, 1.000	0.555, 1.000	0.749, 1.185
Crystal size (mm^3)	0.08 × 0.05 × 0.02	0.30 × 0.015 × 0.01	0.26 × 0.045 × 0.01	0.74 × 0.18 × 0.16
θ(max) (°)	68.2	27.5	27.5	20.0
Reflections measured	68 070	12 337	47 911	51 064
Unique reflections	16 805	12 337	12 466	8583
R_{int}	0.107	0.067	0.056	0.143
Number of parameters	1127	604	556	1129
R_1 [$F^2 > 2\sigma(F^2)$]	0.070	0.061	0.088	0.057
wR_2 (all data)	0.178	0.164	0.168	0.123
GOOF, S	1.011	1.049	1.050	0.913
Largest difference peak and hole (e Å^{-3})	1.42 and −0.86	1.53 and −0.80	0.90 and −1.61	0.30 and −0.25

Compound	**5**·2MeCN	**6**·2MeCN	**7**·2C_3H_6O	**8**·3MeCN
Formula	$C_{56}H_{58}Br_3Cu_2N_6O_2$	$C_{52}H_{54}Br_4CoN_4O_2$·2(C_2H_3N)	$C_{42}H_{30}Br_2Co_2N_4O_4$·2($C_3H_6O$)	$C_{62}H_{65}Br_4Co_2N_{11}O_4$
Formula weight	1213.89	1145.56	1048.56	1465.8
Crystal system	Triclinic	Triclinic	Monoclinic	Monoclinic
Space group	$P\bar{1}$	$P\bar{1}$	$P2_1/c$	Ia
Unit cell dimensions				
a (Å)	10.0808(2)	12.2629(5)	11.4774(8)	15.77810(10)
b (Å)	15.0015(4)	13.2489(6)	14.5787(10)	25.0018(2)
c (Å)	18.6604(5)	17.0384(7)	26.021(3)	16.28380(10)
α (°)	71.442(2)	96.850(3)	90	90
β (°)	82.738(2)	91.115(3)	100.235(8)	91.911(10)
γ (°)	76.600(2)	99.672(4)	90	90
V (Å^3)	2598.2(1)	2707.2(2)	4284.6(6)	6420.08(8)
Z	2	2	4	4
Temperature (K)	100(2)	100(2)	100(2)	100(2)
Wavelength (Å)	1.54184	0.71075	1.54178	0.71073
Calculated density (g cm^{-3})	1.552	1.405	1.535	1.516
Absorption coefficient (mm^{-1})	4.572	3.309	8.652	3.060
T_{min}, T_{max}	0.149, 1.000	0.652, 1.000	0.404, 1.000	0.698, 1.000
Crystal size (mm^3)	0.70 × 0.60 × 0.15	0.10 × 0.04 × 0.02	0.14 × 0.03 × 0.01	0.25 × 0.18 × 0.05
θ(max) (°)	68.3	21.7	68.2	28.7

Table 4 *(Contd.)*

Compound	**5**·2MeCN	**6**·2MeCN	**7**·2C_3H_6O	**8**·3MeCN
Reflections measured	44 092	10 619	6241	147 825
Unique reflections	9337	10 619	3471	16 480
R_{int}	0.083	0.179	0.054	0.047
Number of parameters	622	564	526	762
R_1 [$F^2 > 2\sigma(F^2)$]	0.066	0.114	0.128	0.032
wR_2 (all data)	0.184	0.297	0.371	0.064
GOOF, S	1.062	1.098	1.226	1.023
Largest difference peak and hole (e Å^{-3})	3.45 and −1.24	1.02 and −1.54	2.52 and −2.02	0.52 and −0.46

Compound	**9**	**10**·2MeCN	**11**·2MeCN	**12**·2MeCN	**13**
Formula	$C_{20}H_{30}Br_6Co_3N_{10}$	$C_{28}H_{32}Br_2Co_2N_2O_6{\cdot}2(C_2H_3N)$	$C_{36}H_{44}Br_6Co_4N_6O_6$	$C_{32}H_{38}Br_2Fe_2N_4O_6$	$C_{12}H_{18}Br_6Fe_3N_6O$
Formula weight	1066.79	852.34	1371.95	846.18	909.33
Crystal system	Monoclinic	Triclinic	Triclinic	Triclinic	Trigonal
Space group	$P2_1/n$	$P\bar{1}$	$P\bar{1}$	$P\bar{1}$	$R\bar{3}$:H
Unit cell dimensions					
a (Å)	8.34720(10)	8.4718(5)	10.416(2)	8.51990(10)	12.39520(10)
b (Å)	18.8457(3)	9.2109(3)	11.156(4)	9.20980(10)	12.39520(10)
c (Å)	12.5811(2)	12.2495(5)	11.738(4)	12.1881(2)	30.5277(3)
α (°)	90	101.186(3)	78.04(3)	101.2110(10)	90
β (°)	108.941(2)	102.715(4)	70.59(2)	102.4660(10)	90
γ (°)	90	97.208(4)	87.78(2)	97.4090(10)	120
V (Å^3)	1871.95(5)	900.47(7)	1257.8(7)	901.29(2)	4061.92(8)
Z	2	1	1	1	6
Temperature (K)	100(2)	100(2)	150(2)	100(2)	100(2)
Wavelength (Å)	0.71075	1.54184	0.71073	1.54184	1.54184
Calculated density (g cm^{-3})	1.893	1.572	1.811	1.559	2.230
Absorption coefficient (mm^{-1})	7.743	10.197	6.105	9.433	23.225
T_{min}, T_{max}	0.154, 0.733	0.423, 1.000	0.725, 0.820	0.646, 1.000	0.154, 0.733
Crystal size (mm^3)	0.216 × 0.125 × 0.10	0.32 × 0.16 × 0.10	0.31 × 0.13 × 0.09	0.30 × 0.20 × 0.10	0.16 × 0.14 × 0.03
θ(max) (°)	27.49	68.2	29.2	70.3	67.8
Reflections measured	48 302	15 481	11 602	32 046	24 700
Unique reflections	4301	3240	6632	3387	1644
R_{int}	0.0235	0.066	0.044	0.0342	0.0363
Number of parameters	183	217	268	217	88
R_1 [$F^2 > 2\sigma(F^2)$]	0.017	0.042	0.035	0.0299	0.0188
wR_2 (all data)	0.0037	0.119	0.072	0.0822	0.0474
GOOF, S	1.170	1.072	0.823	1.091	1.111
Largest difference peak and hole (e Å^{-3})	0.79 and −0.35	0.85 and −0.83	0.84 and −0.63	0.413 and −0.69	0.38 and −0.51

were quenched with wet $CDCl_3$. The percent conversion of monomer to polymer was determined by ^1H NMR spectroscopy.

Mass spectrometry

Polymer samples were run at the University of Hull using MALDI-TOF MS analysis. Samples were dissolved in THF, and the matrix, 2-(4-hydroxyphenylazo) benzoic acid (HPABA) with added NaOAc was employed, which was dissolved in THF to give a saturated solution. 50 μL of the sample solution was then mixed with 50 μL matrix solution, and 1 μL of the mixed solution applied to the sample target. The sample was allowed to dry in air before analysis. The co-poly (δ-VL + *r*-LA) (run 7) sample was analysed by MALDI in positive-linear and reflectron modes, with DCTB matrix and NaOAc additive. The sample was fully soluble in THF at 10 mg mL^{-1}.

X-ray crystallography

Single-crystal X-ray diffraction data for the structures (except for **4** and **11**) were collected at the UK National Crystallography service on a range of Rigaku Oxford Diffraction ultra-high intensity instruments employing modern areas detectors. Samples were held at 100 K for data collection. For **4**, data were from a Rigaku Oxford Diffraction Xcalibur-3 CCD diffractometer at 140 K. For **11**, data were from a Stoe IPSD2 image plate diffractometer utilising monochromated Mo radiation (λ = 0.71073 Å). In all cases standard procedures were employed for integration and processing of data. Crystallographic data for all samples are collated in Table 4.

Crystal structures were solved using direct methods (in SHELXS[19a]) or dual space methods implemented within SHELXT.[19b] Completion of structures was achieved by performing least squares refinement against all unique F^2 values using SHELXL-2018.[20] All non-H atoms were refined with anisotropic displacement parameters. Hydrogen atoms were placed using a riding model. Where the location of hydrogen atoms was obvious from difference Fourier maps, C–H and O–H bond lengths were refined subject to chemically sensible restraints. Minor disorder was treated using standard methods.

The crystal of **5** examined was the best of those available. The crystal was split and intensity data from the major component were used for refinement. The final refinement has good quality of fit (R_1 = 6.66%) but it is not perfect because of the imperfect nature of the crystals available.

Conflicts of interest

There are no conflicts of interest to declare.

Acknowledgements

We thank the Chinese Scholarship Council for a PhD studentship (to KW). CR thanks the EPSRC (grant EP/S025537/1) for financial support. We thank the EPSRC National Crystallographic Service at Southampton for data collection and the Physical Sciences Data Service Centre for access to the CCDC. We also thank the National Mass Spectrometry Facility (NMSF), Swansea for data.

References

1 L. M. Heidbreder, I. Bablok, S. Drews and C. Menzel, *Sci. Total Environ.*, 2019, **668**, 1077–1093.
2 (*a*) C. Redshaw, *Catalysts*, 2017, **7**, 165; (*b*) O. Santoro, X. Zhang and C. Redshaw, *Catalysts*, 2020, **10**, 800.
3 (*a*) A. Arbaoui, C. Redshaw and D. L. Hughes, *Chem. Commun.*, 2008, 4717–4719; (*b*) A. Arbaoui, C. Redshaw and D. L. Hughes, *Supramol. Chem.*, 2009, **21**, 35–43; (*c*) W. Yang, K.-Q. Zhao, T. J. Prior, D. L. Hughes, A. Arbaoui, T. Bian, M. R. J. Elsegood and C. Redshaw, *Dalton Trans.*, 2016, **45**, 11990–12005.
4 W. Yang, K.-Q. Zhao, B.-Q. Wang, C. Redshaw, M. R. J. Elsegood, J.-L. Zhao and T. Yamato, *Dalton Trans.*, 2016, **45**, 226–236.
5 K. Wang, T. J. Prior and C. Redshaw, *Chem. Commun.*, 2019, **55**, 11279–11282.
6 F. H. Allen, *Acta Crystallogr., Sect. B: Struct. Sci.*, 2002, **58**, 380–388.
7 (*a*) S. Brooker, *Coord. Chem. Rev.*, 2001, **222**, 33–56; (*b*) W. Radecka-Paryzek, V. Patroniak and J. Lisowski, *Coord. Chem. Rev.*, 2005, **249**, 2156–2175.
8 For examples of iron-based ROP systems see: (*a*) B. J. O'Keefe, S. M. Monnier, M. A. Hillmyer and W. B. Tolman, *J. Am. Chem. Soc.*, 2001, **123**, 339–340; (*b*) B. J. O'Keefe, L. E. Breyfogle, M. A. Hillmyer and W. B. Tolman, *J. Am. Chem. Soc.*, 2002, **124**, 4384–4393; (*c*) K. R. Delle Chiaie, A. B. Biernesser, M. A. Ortuño, B. Dereli, D. A. Iovan, M. J. T. Wilding, B. Li, C. J. Cramer and J. A. Byers, *Dalton Trans.*, 2017, **46**, 12971–12980; (*d*) S.-L. Lee, F.-L. Hu, X.-J. Shang, Y.-X. Shi, A. L. Tan, J. Mizera, J. K. Clegg, W.-H. Zhang, D. J. Young and J.-P. Lang, *New J. Chem.*, 2017, **41**, 14457–14465; (*e*) E. Fazekas, G. S. Nichol, J. A. Garden and M. P. Shaver, *ACS Omega*, 2018, **3**, 16945–16953; (*f*) M. Cozzolino, V. Leo, C. Tedesco, M. Mazzeo and M. Lamberti, *Dalton Trans.*, 2018, **47**, 13229–13238; (*g*) M. A. Ortuño, B. Dereli, K. R. D. Chiaie, A. B. Biernesser, M. Qi, J. A. Byers and C. J. Cramer, *Inorg. Chem.*, 2018, **57**, 2064–2071.
9 A. W. Addison, T. N. Rao, J. Reedijk, G. C. van Rijn and J. Verschoor, *J. Chem. Soc., Dalton Trans.*, 1984, **7**, 1349–1356.
10 For examples of copper-based ROP systems see: (*a*) A. Routaray, N. Nath, T. Maharana and A. K. Sutar, *J. Macromol. Sci., Part A: Pure Appl. Chem.*, 2015, **52**, 444–453; (*b*) M. Mandal, K. Oppelt, M. List, I. Teasdale, D. Chakraborty and U. Monkowius, *Chem. Mon.*, 2016, **147**, 1883–1892; (*c*) M. Zikode, S. O. Ojwach and M. P. Akerman, *Appl. Organomet. Chem.*, 2017, **31**, e3556; (*d*) J. Rueda-Espinosa, J. F. Torres, C. V. Gauthier, L. Wojtas, G. Verma,

M. A. Macias and J. Hurtado, *ChemistrySelect*, 2017, **2**, 9815–9821.

11 For examples of cobalt-based ROP systems see: (*a*) H. J. Jeon, Y. C. You and J. H. Youk, *J. Polym. Sci., Part A: Polym. Chem.*, 2009, **47**(12), 3078–3085; (*b*) J. Zhang, B. Wang, L. Wang, J. Sun, Y. Zhang, Z. Cao and Z. Wu, *Appl. Organomet. Chem.*, 2018, **32**, e4077; (*c*) P. Marin, M. J.-L. Tschan, P. Haquette, T. Roisnel, I. del Rosal, L. Maron and C. M. Thomas, *Eur. Polym. J.*, 2019, **120**, 109208; (*d*) H. C. Pradhan, S. Mantri, A. Routaray, T. Maharaba and A. K. Sutar, *J. Chem. Sci.*, 2020, **132**, 25–31; (*e*) N. Shen, F. Tian, J. Chang, K. L. Huang, Z. H. Zhang, X. Feng, J. Gu, S. C. Chen, M. Y. He and Q. Chen, *CrystEngComm*, 2020, **22**, 3656–3663.

12 (*a*) Z. Zhong, P. J. Dijkstra and J. Feijen, *J. Am. Chem. Soc.*, 2003, **125**, 11291–11298; (*b*) R. M. Slattery, A. E. Stahl, K. R. Brereton, A. L. Rheingold, D. B. Green and J. M. Fritsch, *J. Polym. Sci., Part A: Polym. Chem.*, 2019, **57**, 48–59.

13 R. S. Drago, M. J. Desmond, B. B. Corden and K. A. Miller, *J. Am. Chem. Soc.*, 1983, **105**, 2287–2296.

14 J. J. Randell, C. E. Lewis and P. M. Slagan, *J. Org. Chem.*, 1962, **27**, 4098–4101.

15 V. C. Gibson, C. Redshaw, W. Clegg, M. R. J. Elsegood, U. Siemeling and T. Türk, *Polyhedron*, 2004, **23**, 189–194.

16 B. Weber and E. Kaps, *Heteroat. Chem.*, 2005, **16**, 391–397.

17 M. Kato, H. B. Jonassen and J. C. Fanning, *Chem. Rev.*, 1964, **64**, 99–128.

18 (*a*) R. W. Handel, H. Willms, G. B. Jameson, K. J. Berry, B. Moubaraki, K. S. Murray and S. Brooker, *Eur. J. Inorg. Chem.*, 2010, **2010**(21), 3317–3327; (*b*) A. A. Abou-Hussein and W. Linert, *Spectrochim. Acta, Part A*, 2015, **141**, 223–232.

19 (*a*) G. M. Sheldrick, *Acta Crystallogr., Sect. A: Found. Adv.*, 2008, **64**, 112–122; (*b*) G. M. Sheldrick, *Acta Crystallogr., Sect. A: Found. Adv.*, 2015, **71**, 3–8.

20 G. M. Sheldrick, *Acta Crystallogr., Sect. C: Struct. Chem.*, 2015, **71**, 3–8.